Nonlinear control of wind energy conversion system based on DFIG with a mechanical torque observer

Noussi, K.; Abouloifa, A.; Katir, H.; Lachkar, I.; Giri, F.; Guerrero, J. M.

Link to publication from Aalborg University

Nonlinear Control of Wind Energy Conversion System Based on DFIG with a Mechanical Torque Observer

K. Noussi [*], **A. Abouloifa** [*], **H. Katir** [*], **I. Lachkar** [**], **F. Giri** [***] and **J. M.Guerrero** [****]

[*] LTI Lab, Faculty of Sciences Ben M'sik, University Hasan II of Casablanca, BP 7955 Casablanca, Morocco (e-mail: karim.noussi2@gmail.com).

[**] ESE Lab, ENSEM of Casablanca, University Hasan II of Casablanca, BP 7955 Casablanca, Morocco

[***] Normandie UNIV, UNICAEN, ENSICAEN, LAC, 14000 Caen, France

[****] Department of Energy Technology, AAU, 9220 Aalborg East, Denmark

Abstract: In this paper, an advanced nonlinear backstepping control approach is developed and applied to the whole nonlinear system including the AC/DC/AC converters combined with the doubly-fed induction generator(DFIG). A high gain observer is synthesized, in order to provide an estimated value of the mechanical torque whereas, a wind speed estimation block is designed based on roots polynomial method; followed by sensorless maximum power point tracking (MPPT). The control objectives are fourfold: (i) Forcing the generator speed to track the reference signal given by the MPPT block, (ii) adjusting the stator reactive power injected into the grid to be null, (iii) Regulating the DC-link voltage between the rotor side and the grid side converters at the desired level, (iv) assuring a unitary power factor in the grid side. The achievement of these control objectives leans on a multi-loop regulator which shows a satisfying performance as far as it concerns the simulation results.

Keywords: variable speed wind turbine, doubly-fed induction generator(DFIG), high gain observer, backstepping control.

1. INTRODUCTION

Nowadays, renewable energy sources have come up to fulfill the energy needs and to replace usual electrical sources because of the huge human society consumes of electricity. Wind energy generation has been under the spots since it produces safer energy and being the most penetrating source into the power source supply among all renewable energy sources (Stiebler (2008));(Boussairi et al. (2018)). Most of the major wind turbine manufacturers are developing new larger turbines based on either synchronous generators or doubly-fed induction generators (DFIGs), this last has undoubtedly arisen as one of the leading technologies (Kaloi et al. (2016)). The main advantage of the DFIG that it is a cost-effective, efficient, and reliable solution, where only (20-30 %) of the wind turbine power is flowing throughout the associated power electronic converters (Xiong et al. (2017)).

In this work, the complete chain of the wind energy generation system based on doubly fed induction generator shown in Fig. 1 below is considered, the adopted configuration consists of a back-to-back converter which includes two identical power converters on the rotor side (RSC) and the grid side (GSC) that are linked through a DC-link capacitor. The stator winding of the DFIG is connected directly to the grid, and the rotor winding is connected to the grid via the back-to-back converter.

Most control systems of wind turbines necessit online measurement of mechanical quantities, therfore, mechanical sensors are used, which increase the cost and reduce the reliability of the global system (Qiao et al. (2008)). In this work a high gain observer is used to provide an accurate estimated value of the mechanical torque, and the roots of the power coefficient polynomial approximation are used to elaborate online estimation of the wind speed using the mechanical torque observed value and the generator speed. Addressing the nonlinear control problem of the whole system is rarely found in literature. Many research papers discuss the regulation of the DFIG with the AC/DC converter, which prevents witnessing the performance of the entire architecture. In (Yang et al. (2018));(Villanueva et al. (2017)), sliding mode control simulation results for the DFIG-AC/DC system are investigated. However, authors did not mention any information about the the influence of the powers exchanged with the grid via the GSC. On the other hand, studies on the control of the entire system are still lacking. PI control for DFIG-AC/DC/AC system has been presented in (El Azzaoui and Mahmoudi (2015)). In fact, there are certain drawbacks associated with the use of this suggested approach, the optimal control remains difficult to establish, as long as the accurate machine parameters are necessary (Katir et al. (2019)).

This work presents the modeling and the nonlinear control of the DFIG for the wind energy conversion system. This paper is organized in sections, where the modeling of the wind turbine based on the DFIG connected to the AC/DC/AC converters is established in sect 2. Stability analysis of the high gain observer and wind speed computation are shown in sect 3. A backstepping controller is developed in sect 4 to adjust the generator speed and the stator reactive power acting on the RSC as well as to maintain the DC-link voltage and the grid reactive power at a well defined constant value taking action on the GSC. Finally, the obtained simulation results, performed in Matlab/Simulink SimPowerSystems environment, are presented and discussed in sect 5.
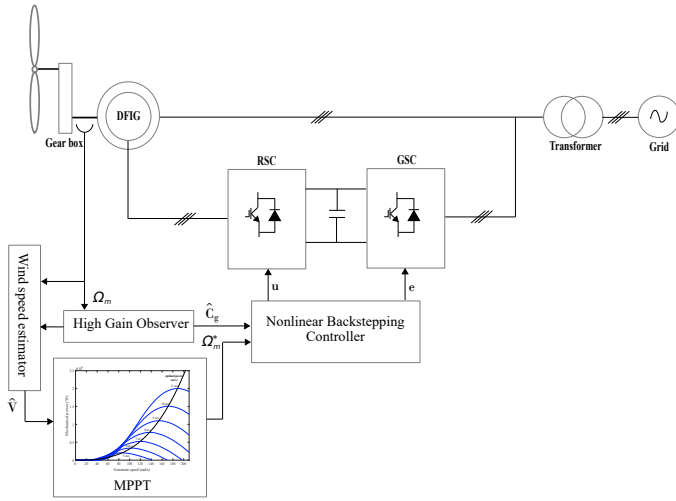

Fig. 1. Simplified scheme of the DFIG wind turbine.

2. SYSTEM MODELING

2.1 Wind turbine modeling

The amount of mechanical power available in the wind turbine rotor, by converting the captured kinetic energy in the wind, is given by the following expression:

$$P_t = C_t \Omega_t = \frac{1}{2}\rho\pi R^2 v^3 C_p(\lambda, \beta) \qquad (1)$$

where C_t, Ω_t, ρ, R, v, C_p are the aerodynamic toque, the rotor angular speed, the air density, the rotor radius, the wind speed and the power coefficient, respectively.
The tip speed ratio has been expressed by the following equation:

$$\lambda = \frac{\Omega_t R}{v} \qquad (2)$$

For the variable speed wind turbine, the approximated power coefficient value of the turbine rotor is given by the following expression:

$$C_p(\lambda, \beta) = C_1(\frac{C_2}{\lambda_i} - C_3\beta - C_4\beta^{C_5} - C_6)e^{(\frac{-C_7}{\lambda_i})} \qquad (3)$$

with

$$\frac{1}{\lambda_i} = \frac{1}{\lambda + 0.02\beta} - \frac{0.003}{\beta^3 + 1} \qquad (4)$$

where the coefficients C_i have the numerical values given by Table 1.

2.2 DFIG dynamic model

Different variable speed wind turbine (VSWT) designs are used; the doubly-fed induction generator coupled to a wind turbine is common, robust, and efficient. The equations of the stator and rotor voltage space vectors in the d-q reference frame of the DFIG machine can be described as follows:

$$\vec{v}_s^{dq} = R_s \vec{i}_s^{dq} + \frac{d\vec{\phi}_s^{dq}}{dt} + j\omega_s \vec{\phi}_s^{dq} \qquad (5a)$$

$$\vec{v}_r^{dq} = R_r \vec{i}_r^{dq} + \frac{d\vec{\phi}_r^{dq}}{dt} + j\omega_r \vec{\phi}_r^{dq} \qquad (5b)$$

where $\vec{v}_s^{dq}$, $\vec{v}_r^{dq}$ are the space vectors of the stator and rotor voltages in the d-q reference frame; $\vec{i}_s^{dq}$, $\vec{i}_r^{dq}$ denote the space vectors of the stator and rotor currents in the synchronous reference frame, respectively; R_s, R_r are the stator and the rotor resistance; ω_s, ω_m, ω_r are respectively the synchronous speed of stator flux, the angular rotor speed and the rotor angular frequency, with $\omega_r = \omega_s$ - ω_m. The equations of the stator and the rotor fluxes space vectors in the d-q reference frame are given by:

$$\vec{\phi}_s^{dq} = L_s \vec{i}_s^{dq} + M \vec{i}_r^{dq} \qquad (6a)$$

$$\vec{\phi}_r^{dq} = L_r \vec{i}_r^{dq} + M \vec{i}_s^{dq} \qquad (6b)$$

where L_s, L_r and M denote respectively the stator, rotor leakage and the mutual inductance.
The expression of the shaft system dynamics is given by:

$$J\frac{d\Omega_m}{dt} = C_g - C_{em} - F.\Omega_m \qquad (7)$$

where Ω_m, C_g, J, F are the DFIG mechanical rotational speed, mechanical torque, the rotor inertia and the friction coefficient, respectively.
with $\Omega_t = \Omega_m/N$ and $C_t = C_g.N$, where N is the gear box gain.
The electromagnetic torque and stator reactive power expressed in the d-q coordinates are given by:

$$C_{em} = \frac{3}{2}(v_{sq}i_{sd} - v_{sd}i_{sq}) \qquad (8)$$

$$Q_s = \frac{3pM}{2L_s}(i_{rd}\phi_{sq} + i_{rq}\phi_{sd}) \qquad (9)$$

The field-oriented strategy is applied to simplify the state space of the controlled system. To reach this goal, the stator flux has been adjusted to be aligned with the d-axis ($v_{sd} = \phi_{sq} = 0$, $v_{sq} = V_s = \omega_s.\phi_{sd}$). Therefore, the stator reactive power is controlled by the direct current and the electromagnetic torque is directly controlled by the quadrature current.

$$C_{em} = -\frac{3pM}{2L_s}.\phi_{sd}.i_{rq} \qquad (10)$$

$$Q_s = -\frac{3\omega_s M}{2L_s}\phi_{sd}.(i_{rd} - \frac{\phi_{sd}}{M}) \qquad (11)$$

2.3 GSC system dynamic model

The grid side system includes the grid side converter, a filter and the grid power supply.

The same idea of the field-oriented strategy previously mentionned is also applied to the GSC. Hence, a decoupled relationship between the active and the reactive power has been achieved (Noussi et al. (2019)).

$$\frac{dv_{dc}^2}{dt} = \frac{-3V_s}{C}i_{gq} + \frac{2}{C}V_{dc}.i_r \tag{12a}$$

$$\frac{di_{gq}}{dt} = \frac{v_{dc}}{2L_g}e_q - \omega_s i_{gd} - \frac{V_s}{L_g} \tag{12b}$$

$$\frac{di_{gd}}{dt} = \frac{v_{dc}}{2L_g}e_d + \omega_s i_{gq} \tag{12c}$$

where v_{dc}, i_r, i_{gd}, i_{gq} are the DC-link voltage, the current flowing from the RSC to the DC-link and the dq-axis grid currents, respectively.

The grid side reactive power exchanged with the grid is described by:

$$Q_g = \frac{3}{2}V_s.i_{gd} \tag{13}$$

3. HIGH-GAIN OBSERVER AND WIND SPEED ESTIMATOR

3.1 High-gain observer

The present sub-section aims at designing a high gain observer, which provides an estimated value of the mechanical torque to be used in designing the proposed regulator. The design of the suggested high gain observer is based on equation (7), which can be rewritten as:

$$\dot{w} = Gw + \Psi(w,\nu) + \Lambda(t) \tag{14a}$$

$$y = Cx \tag{14b}$$

where

$$w = [w_1, w_2]^T = [\Omega_m, \frac{C_g}{J}]^T; \quad \nu = C_{em} \tag{15}$$

$$G = \begin{bmatrix} 0 & 1 \\ 0 & 0 \end{bmatrix}; \quad \Psi(w,\nu) = \begin{bmatrix} \frac{-Fw_1 - \nu}{J} \\ 0 \end{bmatrix} \tag{16}$$

$$\Lambda(t) = \begin{bmatrix} 0 \\ f(t) \end{bmatrix}; \quad C = [1 \ 0] \tag{17}$$

The proposed observer for system (14) can be given as follows:

$$\dot{\widehat{w}} = G\widehat{w} + \Psi(\widehat{w},\nu) - \theta\Delta_\theta^{-1}S^{-1}C^T(C\widehat{w} - y) \tag{18}$$

where

$$\Delta_\theta = \begin{bmatrix} 1 & 0 \\ 0 & \frac{1}{\theta} \end{bmatrix}, \quad with \ \theta > 0. \tag{19}$$

3.2 Wind speed estimation

In this sub-section, a calculation of the estimated wind speed value is discussed. Substituting equation (2) in (1), the power coefficient can be rewritten as a function of the aerodynamic torque, the rotor speed and the tip speed ratio:

$$C_p(\widehat{\lambda}) = \frac{2N\widehat{C_t}\widehat{\lambda}^3}{\rho\pi R^5\Omega_t^2} \tag{20}$$

Using MATLAB/SIMULINK digital tools, a polynomial approximation of equation (3) for a fixed value of β, which
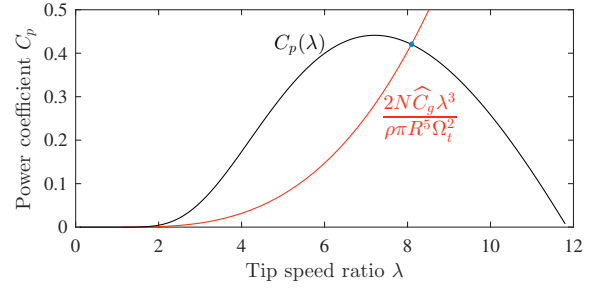

Fig. 2. The shapes of the power coefficient and the equation (20) as a function of the tip speed ratio.

is discussed in the following section, can be constructed as follows:

$$C_p(\lambda) = h_3\lambda^3 + h_2\lambda^2 + h_1\lambda + h_0. \tag{21}$$

The power coefficient constants are illustrated in Table 1. The intersection point of equation (20) and (21) as shown in Fig. 2, represents the value of the tip speed ratio. The online resolution of this equality gives an estimated value of the tip speed ratio to be used in equation (2) in order to estimate the wind speed.

4. CONTROLLER DESIGN

4.1 Power capture optimisation

To optimize the aerodynamic performance, the power coefficient $C_p(\beta,\lambda)$ should be maintained at its optimal value C_p^{opt}, for this reason and according to power coefficient curve for different pitch angles the tip speed ratio λ and the pitch angle β are fixed to their optimal values $\beta = \beta_{opt}$ and $\lambda = \lambda_{opt}$ (Bektache and Boukhezzar (2018)).

Wind turbine operates in four operation zones, the main objective of the speed control in zone 2 is to extract the maximum power. To achieve this objective the generator
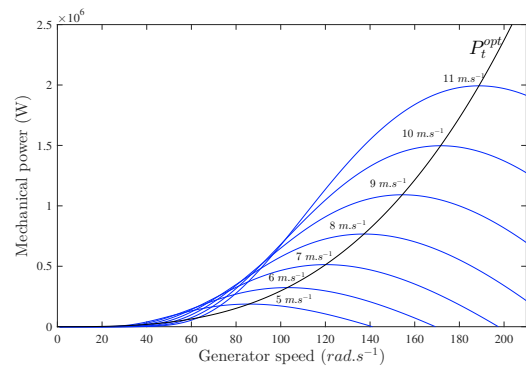
Fig. 3. The shape of the aerodynamic power as a function of the generator speed for differents wind speed values.

speed should follow the optimal reference for given wind speed to extract the maximum mechanical power and inject this last to the grid through the DFIG-AC/DC/AC system.

Fig. 3 shows the optimal power which can be captured for different Ω_m and the mechanical power as a function of Ω_m for different wind values. The intersection couples (Ω_m, v) of the optimal power P_t^{opt} and $P_t(\Omega_m, v)$ represent the unique maximum power value. The intersection data

in Fig. 3 are collected and interpolated to construct a polynomial function represented by:

$$\Omega_m^* = a_4 v^4 + a_3 v^3 + a_2 v^2 + a_1 v + a_0. \qquad (22)$$

The reference speed function constants are illustrated in Table 1.

4.2 Controller design

The main control objectives in this work are:

• Speed regulation: forcing the generator speed to track, as closely as possible, the reference speed given by the MPPT strategy.

• Stator reactive power regulation: maintain the stator reactive power injected into the grid at the suggested reference.

• DC-link voltage regulation: the DC-link voltage must be regulated at a well-defined constant value v_{dc}^*, its set to the nominal voltage to protect the rotor side converter from damage.

• Power factor correction: assuring a unitary power factor, to reach this goal the grid reactive power must be driven to zero.

The average model of the whole system involving the AC/DC/AC converters combined with the DFIG machine is then given in the following form:

$$\dot{x}_1 = -\frac{3pM}{2JL_s}\phi_{sd}x_2 - \frac{1}{J}C_g - \frac{F}{J}x_1 \qquad (23a)$$

$$\dot{x}_2 = \frac{1}{\sigma L_r}\left(\frac{\sqrt{x_4}}{2}v_q - R_r x_2 - \omega_r \sigma L_r x_3 - g\frac{MV_s}{L_s}\right) (23b)$$

$$\dot{x}_3 = \frac{1}{\sigma L_r}\left(\frac{\sqrt{x_4}}{2}v_d - R_r x_3 + \omega_r \sigma L_r x_2\right) \qquad (23c)$$

$$\dot{x}_4 = -\frac{3V_s}{C}x_5 + \frac{2\sqrt{x_4}}{C}i_r \qquad (23d)$$

$$\dot{x}_5 = \frac{\sqrt{x_4}}{2L_g}e_q - \omega_s x_6 - \frac{V_s}{L_g} \qquad (23e)$$

$$\dot{x}_6 = \frac{\sqrt{x_4}}{2L_g}e_d + \omega_s x_5 \qquad (23f)$$

where $x_1, x_2, x_3, x_4, x_5, x_6$ are the mean values, over cutting periods, of the real signals $\Omega_m, i_{rq}, i_{rd}, v_{dc}^2, i_{gd}, i_{gq}$, respectively.

Let us consider that the dynamic behaviour of the observer is fast enough regarding the closed loop system dynamic behaviour, therefore, confusion between the actual and estimated values of C_g occurs during the control law synthesis, consequently the mechanical torque is replaced by its estimated value $\widehat{C}_g$.

Generator speed regulator:

The generator speed must track its reference x_1^*, let us define the speed tracking error z_1 as:

$$z_1 = x_1 - x_1^* \qquad (24)$$

Step 1:
Using (23a), the dynamic of equation (24) can be expressed as:

$$\dot{z}_1 = \frac{-3pM}{2JL_s}\phi_{sd}x_2 - \frac{1}{J}\widehat{C}_g - \frac{F}{J}x_1 - \dot{x}_1^* \qquad (25)$$

The first Lyapunov candidate function is chosen such that:

$$V_1(z) = \frac{1}{2}z_1^2 \qquad (26)$$

To make the speed tracking error tends to zero, the derivative of the candidate Lyapunov function must be always negative.

$$\dot{V}_1(z) = -c_1 z_1^2, \quad where \;\; c_1 > 0 \qquad (27)$$

Using (25), (27) and the dynamics of (26), one can easily get the following stabilizing function:

$$x_2^* = \frac{-2JL_s}{3pM\phi_{sd}}\left(-c_1 z_1 + \frac{1}{J}\widehat{C}_g + \frac{F}{J}x_1 + \dot{x}_1^*\right) \qquad (28)$$

As x_2^* is not the actual control input, one defines the second tracking error of the current as:

$$z_2 = x_2 - x_2^* \qquad (29)$$

Using (28) and (29), one gets from (25):

$$\dot{z}_1 = -c_1 z_1 - \frac{3pM}{2JL_s}\phi_{sd}z_2 \qquad (30)$$

Substituting (30) in the dynamics of (26), one obtains:

$$\dot{V}_1(z) = -c_1 z_1^2 - \frac{3pM}{2JL_s}\phi_{sd}z_1 z_2 \qquad (31)$$

Step 2:
The time derivative of equation (29) can be expressed as follows:

$$\dot{z}_2 = \frac{1}{\sigma L_r}\left(\frac{\sqrt{x_4}}{2}v_q - R_r x_2 - \underbrace{(\omega_r \sigma L_r x_3 + g\frac{MV_s}{L_s})}_{\alpha_d}\right) - \dot{x}_2^* \qquad (32)$$

Considering the augmented Lyapunov candidate function:

$$V_2(z) = V_1(z) + \frac{1}{2}z_2^2 \qquad (33)$$

As in the previous step, one must choose the derivative of the Lyapunov function to be always negative as well

$$\dot{V}_2(z) = -c_1 z_1^2 - c_2 z_2^2, \quad where \;\; c_2 > 0 \qquad (34)$$

Comparing the time derivative of (33) to (34) yields:

$$\dot{z}_2 = -c_2 z_2 + \frac{3pM}{2JL_s}\phi_{sd}z_1 \qquad (35)$$

Using (32) and (35), one can derive the following control law:

$$v_q = \frac{2}{\sqrt{x_4}}\left((R_r x_2 + \alpha_d) + \sigma L_r(\dot{x}_2^* - c_2 z_2 + \frac{3pM}{2JL_s}\phi_{sd}z_1)\right) \qquad (36)$$

Stator reactive power regulator:

In this loop, the regulation of the stator reactive power is considered. In order to reach a satisfying unity power factor, the reactive power Q_s should be null.

Let us introduce z_3, the tracking error of the stator reactive power:

$$z_3 = Q_s - Q_s^* \qquad (37)$$

Using (11) and (23c), the time derivative of (37) is given by:

$$\dot{z}_3 = -\frac{3\omega_s M}{2\sigma L_r L_s}\phi_{sd}.\left(\frac{\sqrt{x_4}}{2}v_d - R_r x_3 + \omega_r \sigma L_r x_2\right) - \dot{Q}_s^* \quad (38)$$

The third Lyapunov candidate function is selected such that $V_3 = \frac{1}{2}z_3^2$ and its time derivative must be negative

$\dot{V}_3(z) = -c_3 z_3^2$, where $c_3 > 0$, hence the error tends to zero.

From the above equations, one deduces that:

$$v_d = \frac{2}{\sqrt{x_4}} \left(\frac{-2\sigma L_r L_s}{3\omega_s M \phi_{sd}} (-c_3 z_3 + \dot{Q}_s^*) + R_r x_3 - \omega_r \sigma L_r x_2 \right)$$ (39)

DC-link voltage regulator:

The objective of this control loop is to ensure the regulation of the squared DC-link voltage to the squared desired reference .

Step 1:

Choose $z_4 = x_4 - x_4^*$, and using (23d), one can assert that:

$$\dot{z}_4 = \underbrace{-\frac{3V_s}{C} x_5}_{\mu_1} + \underbrace{\frac{2\sqrt{x_4}}{C} i_r - \dot{x}_4^*}_{\eta_1}$$ (40)

Let us assume μ_1 to be the virtual control input for the error z_4 and the Lyapunov candidate function is considered as $V_4 = \frac{1}{2} z_4^2$, its time derivative $\dot{V}_4(z) = -c_4 z_4^2$, where $c_4 > 0$, following the method of backstepping it is easily seen that the virtual control input can be writing as follow:

$$\mu_1^* = -c_4 z_4 - \eta_1$$ (41)

As μ_1 is not the actual control input, one define the error on the current in order to obtain a stabilizing control law:

$$z_5 = \mu_1 - \mu_1^*$$ (42)

Step 2:

Using (23e), the dynamic of (42) can be expressed as:

$$\dot{z}_5 = -\frac{3V_s \sqrt{x_4}}{2CL_g} e_q + \underbrace{\frac{3\omega_s V_s}{CL_g} x_6 + \frac{3V_s^2}{CL_g} - \dot{\mu}_1^*}_{\eta_2}$$ (43)

And, to elaborate the control law Considering the augmented Lyapunov candidate function:

$$V_5(z) = V_4(z) + \frac{1}{2} z_5^2$$ (44)

Its time derivative along the trajectory of (z_4, z_5) :

$$\dot{V}_5(z) = -c_4 z_4^2 + z_5(z_4 + \dot{z}_5)$$ (45)

$\dot{V}_5(z)$ must be negative, to this end consider $\dot{V}_5(z) = -c_4 z_4^2 - c_5 z_5^2$, with this choice and using (45) we can easily check that:

$$\dot{z}_5 = -c_5 z_5 - z_4$$ (46)

Using (43) and (46), the control law can be expressed as follows:

$$e_q = \frac{2CL_g}{3V_s \sqrt{x_4}} (z_4 + c_5 z_5 + \eta_2)$$ (47)

Grid side reactive power regulator:

In this loop, the reactive power Q_g is set to zero to guarntee a unity power factor.

Let us introduce the tracking error:

$$z_6 = Q_g - Q_g^*$$ (48)

It follows from (13) and (23f) that the dynamic of (48) can be writing as:

$$\dot{z}_6 = \frac{3V_s \sqrt{x_4}}{4L_g} e_d + \underbrace{\frac{3\omega_s V_s}{2L_g} x_5 - \dot{Q}_g^*}_{\eta_3}$$ (49)

The control law can be writing as:

$$e_d = \frac{-2L_g}{3V_s \sqrt{x_4}} (c_6 z_6 + \eta_3)$$ (50)

Table 1. MPPT parameters.

Parameters	Value
$C_1, C_2, C_3, C_4, C_5, C_6, C_7$	.73, 151, .58, .002, 2.14, 13.2, 18.4
C_p^{opt}, λ_{opt}	0.44, 7.2
a_0, a_1, a_2, a_3, a_4	-25.89, 33.28, -3.56, 0.33, -0.01
h_0, h_1, h_2, h_3	-0.0225, -0.0203, 0.0269, -0.0022

Table 2. Controller parameters.

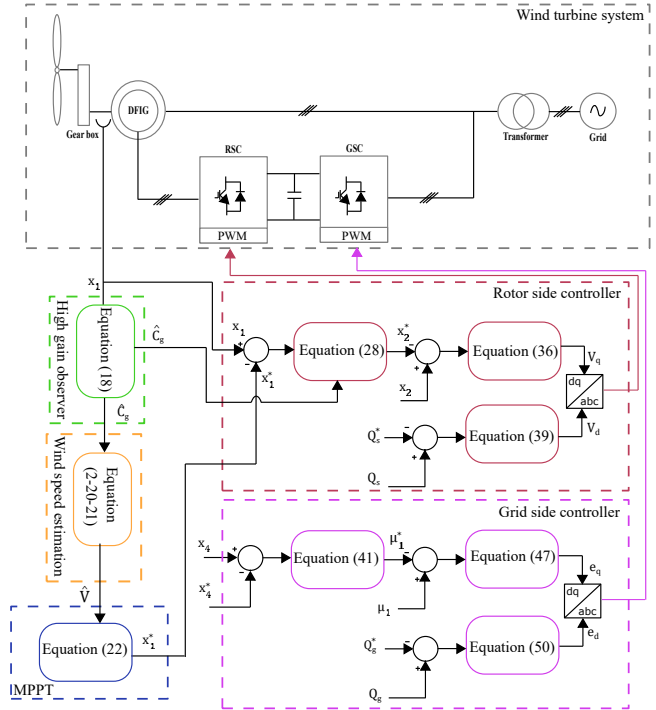|	Parameters	Value
High gain observer	θ	160
Rotor side controller	c_1, c_2, c_3	260,400,310
Grid side controller	c_4, c_5, c_6	1500, 50, 800

Fig. 4. Wind turbine system controller.

Table 3. Wind system turbine parameters.

Parameters	Symbol	Value
Turbine	N	100
	R	42m
	ρ	$1.1225 Kg.m^3$
Supply network voltage	V_n / U_n	400/690V
	f	50Hz
AC/DC/AC converters	L_g	40mH
	C	80mF
DFIG machine	P_n	2MW
	R_s / R_r	$2.6m\Omega/2.9m\Omega$
	L_s / L_r	$26mH/26mH$
	L_m	$2.5mH$

5. SIMULATION

The overall model described by Fig. 4 has been performed using MATLAB/simulink SimPowerSystems environment, the simulation results are obtained by choosing the real parameters of a wind turbine and a 2MW doubly fed induction generator values as shown in table 3.

The simulation results have been obtained under random wind speed with average speed of 8 m/s represented in Fig. 5a. Fig. 5b proves that the high gain observer is

robust and guarantee better performance despite the fast variation of the mechanical torque values. The estimated wind speed tracks well the accurate value as shown in Fig. 5a, therefore the maximum power extraction can be done without measuring the wind speed. As can be seen from Fig. 5c, the power coefficient of the wind turbine is equal to its optimal value, which shows the robustness of the MPPT strategy. Figs. 5d-5i prove the proposed controller's capabilities which confirm the achievement of the control objectives. Figs. 5d and 5e show the robustness of the RSC controller, Fig. 5d illustrates that the generator speed tracks well the reference delivered by the MPPT block and responds to the wind speed variations rapidly. The stator and the grid reactive power produced by the wind turbine achieve the desired value as demonstrated by Figs. 5e and 5g, leading to the achievement of the power factor correction objective as shown in Fig. 5h.

A remarkable transient coming from the start-up of the wind turbine system is depicted in simulation results. In fact, an overvoltage at the DC-link is caused by the high rotor power in transient operation (Fig. 5f). After this latter, the DC-link tracks efficiently the desired fixed value. Fig. 5i represents the global active and reactive powers injected into the grid.
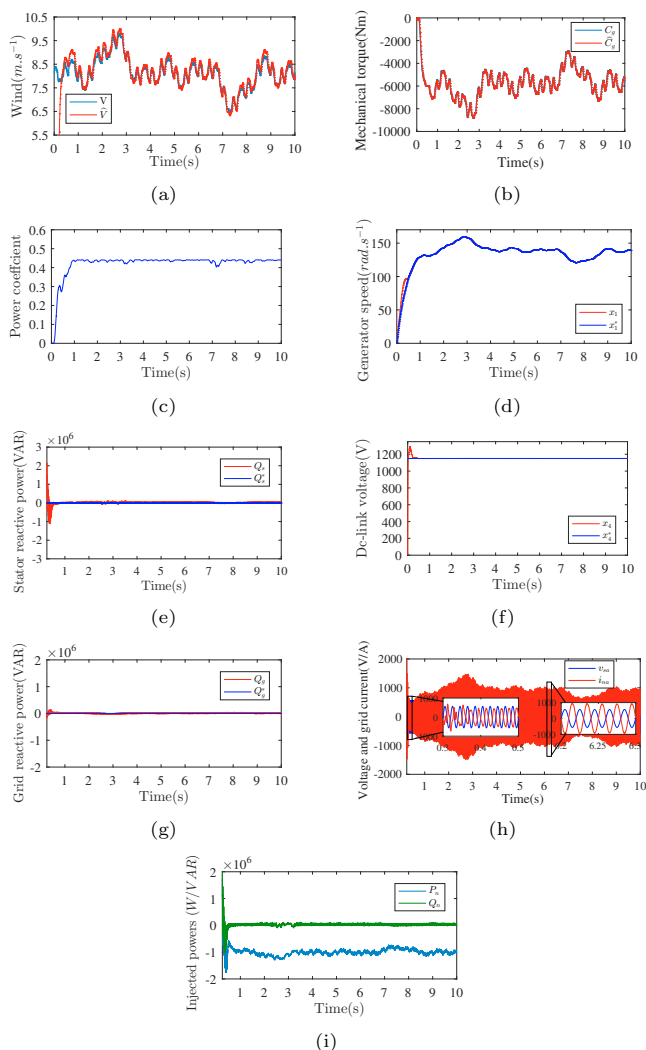

Fig. 5. Wind turbine system simulation results with wind speed variations.

6. CONCLUSION

In this paper, we have proposed a nonlinear backstepping control approach for wind turbine based on the doubly fed induction generator connected to the AC/DC/AC converters. To improve the efficiency of the control system, a high gain observer and roots polynomial method have been considered to estimate the mechanical torque and the wind speed values. It's clearly shown that the control objectives are achieved after using the suggested control techniques.

REFERENCES

Bektache, A. and Boukhezzar, B. (2018). Nonlinear predictive control of a dfig-based wind turbine for power capture optimization. *International Journal of Electrical Power & Energy Systems*, 101, 92–102.

Boussairi, Y., Abouloifa, A., Lachkar, I., Hamdoun, A., and Aouadi, C. (2018). Modeling and nonlinear control of a wind turbine system based on a permanent magnet synchronous generator connected to the three-phase network. *International Journal of Power Electronics and Drive Systems*, 9, 766.

El Azzaoui, M. and Mahmoudi, H. (2015). Modeling and control of a doubly fed induction generator base wind turbine system optimizition of the power. *Journal of Theoretical and Applied Information Technology*, 80(2), 304.

Kaloi, G.S., Wang, J., and Baloch, M.H. (2016). Active and reactive power control of the doubly fed induction generator based on wind energy conversion system. *Energy Reports*, 2, 194–200.

Katir, H., Abouloifa, A., Noussi, K., and Lachkar, I. (2019). Adaptive backstepping control of cascaded h-bridge multilevel dc/ac converters. In *2019 4th World Conference on Complex Systems (WCCS)*, 1–6. IEEE.

Noussi, K., Abouloifa, A., Katir, H., and Lachkar, I. (2019). Modeling and control of a wind turbine based on a doubly fed induction generator. In *2019 4th World Conference on Complex Systems (WCCS)*, 1–5. IEEE.

Qiao, W., Zhou, W., Aller, J.M., and Harley, R.G. (2008). Wind speed estimation based sensorless output maximization control for a wind turbine driving a dfig. *IEEE transactions on power electronics*, 23(3), 1156–1169.

Stiebler, M. (2008). *Wind energy systems for electric power generation*. Springer Science & Business Media.

Villanueva, I., Rosales, A., Ponce, P., and Molina, A. (2017). Stator-flux-oriented sliding mode controller for dfig with variable hysteresis loop for limiting switch frequency of rotor-side power converter. In *2017 IEEE International Conference on Industrial Technology (ICIT)*, 213–218. IEEE.

Xiong, L., Li, P., Li, H., and Wang, J. (2017). Sliding mode control of dfig wind turbines with a fast exponential reaching law. *Energies*, 10(11), 1788.

Yang, B., Yu, T., Shu, H., Dong, J., and Jiang, L. (2018). Robust sliding-mode control of wind energy conversion systems for optimal power extraction via nonlinear perturbation observers. *Applied Energy*, 210, 711–723.